

SIMULATION OF MUTUALLY COUPLED OSCILLATORS USING NONLINEAR PHASE MACROMODELS

DAVIT HARUTYUNYAN, JOOST ROMMES, JAN TER MATEN, AND WIL SCHILDERS

ABSTRACT. Design of integrated RF circuits requires detailed insight in the behavior of the used components. Unintended coupling and perturbation effects need to be accounted for before production, but full simulation of these effects can be expensive or infeasible. In this paper we present a method to build nonlinear phase macromodels of voltage controlled oscillators. These models can be used to accurately predict the behavior of individual and mutually coupled oscillators under perturbation at a lower cost than full circuit simulations. The approach is illustrated by numerical experiments with realistic designs.

1. INTRODUCTION

The design of modern RF (radio frequency) integrated circuits becomes increasingly more complicated due to the fact that more functionality needs to be integrated on a smaller physical area. In the design process floor planning, i.e., determining the locations for the functional blocks, is one of the most challenging tasks. Modern RF chips for mobile devices, for instance, typically have an FM radio, Blue-tooth, and GPS on one chip. Each of these functionalities are implemented with Voltage Controlled Oscillators (VCOs), that are designed to oscillate at certain different frequencies. In the ideal case, the oscillators operate independently, i.e., they are not perturbed by each other or any signal other than their input signal. Practically speaking, however, the oscillators are influenced by unintended (parasitic) signals coming from other blocks (such as Power Amplifiers) or from other oscillators, via for instance (unintended) inductive coupling through the substrate. A possibly undesired consequence of the perturbation is that the oscillators lock to a frequency different than designed for, or show pulling, in which case the oscillators are perturbed from their free running orbit without locking.

Oscillators appear in many physical systems and interaction between oscillators has been of interest in many applications. Our main motivation comes from the design of RF systems, where oscillators play an important role [6, 17, 9, 3] in, for instance, high-frequency phase locked loops (PLLs). Oscillators are also used in the modeling of circadian rhythm mechanisms, one of the most fundamental physiological processes [2]. Another application area is the simulation of large-scale biochemical processes [16].

Date: December 18, 2008.

Key words and phrases. voltage controlled oscillators, pulling, injection locking, phase noise, circuit simulation, behavioral modeling .

This work was supported by EU Marie-Curie project O-MOORE-NICE! FP6 MTKI-CT-2006-042477.

Although the use of oscillators is widely spread over several disciplines, their intrinsic nonlinear behavior is similar, and, moreover, the need for fast and accurate simulation of their dynamics is universal. These dynamics include changes in the frequency spectrum of the oscillator due to small noise signals (an effect known as jitter [6]), which may lead to pulling or locking of the oscillator to a different frequency and may cause the oscillator to malfunction. The main difficulty in simulating these effects is that both phase and amplitude dynamics are strongly nonlinear and spread over separated time scales [15]. Hence, accurate simulation requires very small time steps during time integration, resulting in unacceptable simulation times that block the design flow. Even if computationally feasible, transient simulation only gives limited understanding of the causes and mechanisms of the pulling and locking effects.

To some extent one can describe the relation between the locking range of an oscillator and the amplitude of the injected signal (these terms will be explained in more detail in Section 2). Adler [1] shows that this relation is linear, but it is now well known that this is only the case for small injection levels and that the modeling fails for higher injection levels [14]. Also other linearized modeling techniques [17] suffer, despite their simplicity, from the fact that they cannot model nonlinear effects such as injection locking [14, 20].

In this paper we use the nonlinear phase macromodel introduced in [6] and further developed and analyzed in [14, 15, 20, 8]. Contrary to linear macromodels, the nonlinear phase macromodel is able to capture nonlinear effects such as injection locking. Moreover, since the macromodel replaces the original oscillator system by a single scalar equation, simulation times are decreased while the nonlinear oscillator effects can still be studied without loss of accuracy. We will show how such macromodels can also be used to predict the behavior of inductively coupled oscillators.

Returning to our motivation, during floor planning, it is of crucial importance that the blocks are located in such away that the effects of any perturbing signals are minimized. A practical difficulty here is that transient simulation of the full system is very expensive and usually unfeasible during the early design stages. One way to get insight in the effects of inductive coupling and injected perturbation signals is to apply the phase shift analysis [6]. In this paper we will explain how this technique can be used to estimate the effects for perturbed individual and coupled oscillators. We will consider perturbations caused by oscillators and by other components such as balanced/unbalanced transformers (baluns).

The paper is organized as follows. In Section 2 we summarize the phase noise theory. A practical oscillator model and an example application are described in Section 3. Inductively coupled oscillators are discussed in detail in Section 4. In Section 5 we give an overview of existing methods to model injection locking of individual and resistively/capacitively coupled oscillators. In Section 6 we show how the phase noise theory can be used to analyze oscillator-balun coupling. Numerical results are presented in Section 7 and the conclusions are drawn in Section 8.

2. PHASE NOISE ANALYSIS OF OSCILLATOR

A general free-running oscillator can be expressed as an autonomous system of differential (algebraic) equations:

$$(1a) \quad \frac{d\mathbf{q}(\mathbf{x})}{dt} + \mathbf{j}(\mathbf{x}) = 0,$$

$$(1b) \quad \mathbf{x}(0) = \mathbf{x}(T),$$

where $\mathbf{x}(t) \in \mathbb{R}^n$ are the state variables, T is the period of the free running oscillator, which is in general unknown, and $\mathbf{q}, \mathbf{j} : \mathbb{R}^n \rightarrow \mathbb{R}^n$ are (nonlinear) functions describing the oscillator's behavior. The solution of (1) is called periodic steady state (PSS) and is denoted by \mathbf{x}_{pss} . Although finding the PSS solution can be a challenging task in itself, we will not discuss this in the present paper and refer the interested reader to, for example, [10, 4, 11, 12, 19, 8].

A general oscillator under perturbation can be expressed as a system of differential equations

$$(2a) \quad \frac{d\mathbf{q}(\mathbf{x})}{dt} + \mathbf{j}(\mathbf{x}) = \mathbf{b}(t),$$

$$(2b) \quad \mathbf{x}(0) = \mathbf{x}_{pss}(0),$$

where $\mathbf{b}(t) \in \mathbb{R}^n$ are perturbations to the free running oscillator. For small perturbations $\mathbf{b}(t)$ it can be shown [6] that the solution of (2) can be approximated by

$$(3) \quad \mathbf{x}_p(t) = \mathbf{x}_{pss}(t + \alpha(t)),$$

where $\alpha(t) \in \mathbb{R}$ is called the phase shift. The phase shift $\alpha(t)$ satisfies the following scalar nonlinear differential equation:

$$(4a) \quad \dot{\alpha}(t) = \mathbf{V}^T(t + \alpha(t)) \cdot \mathbf{b}(t),$$

$$(4b) \quad \alpha(0) = 0,$$

with $\mathbf{V}(t) \in \mathbb{R}^n$ being the perturbation projection vector (PPV) [6] of (2) and n is the system size. The PPV is a periodic function with the same period as the oscillator and can efficiently be computed directly from the PPS solution, see for example [5]. Using this simple and numerically cheap method one can do many kinds of analysis for oscillators, e.g. injection locking, pulling, a priori estimate of the locking range [6, 14].

3. LC OSCILLATOR

For many applications oscillators can be modeled as an LC tank with a nonlinear resistor as shown in Fig. 1. This circuit is governed by the following differential equations for the unknowns (v, i) :

$$(5a) \quad C \frac{dv(t)}{dt} + \frac{v(t)}{R} + i(t) + S \tanh\left(\frac{G_n}{S} v(t)\right) = b(t),$$

$$(5b) \quad L \frac{di(t)}{dt} - v(t) = 0,$$

where C , L and R are the capacitance, inductance and resistance, respectively. The nodal voltage is denoted by v and the branch current of the inductor is denoted by i . The voltage controlled nonlinear resistor is defined by S and G_n , where S determines the oscillation amplitude and G_n is the gain.

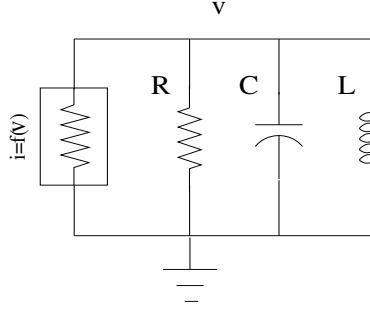
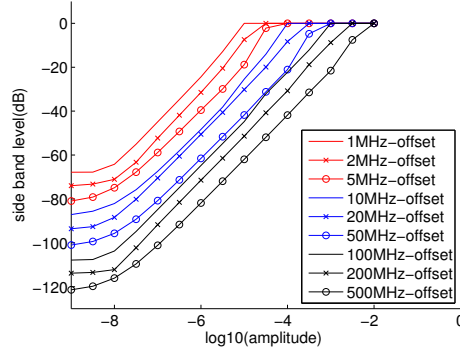
FIGURE 1. Voltage controlled oscillator, $f(v) = S \tanh(\frac{G_n}{S}v(t))$.

FIGURE 2. Side band level of the voltage response versus the injected current amplitude for different offset frequencies.

A lot of work [17, 14] has been done for the simulation of this type of oscillators. Here we will give an example that can be of practical use for designers. During the design process, early insight in the behavior of system components is of crucial importance. In particular, for perturbed oscillators it is very convenient to have a direct relationship between the injection amplitude and the side band level.

For the given RLC circuit with the following parameters $L = 930 \cdot 10^{-12}$ H, $C = 1.145 \cdot 10^{-12}$ F, $R = 1000 \Omega$, $S = 1/R$, $G_n = -1.1/R$ and injected signal $b(t) = A \sin(2\pi f)$, we plot the side band level of the voltage response versus the amplitude A of the injected signal for different offset frequencies, see Fig. 2. We see, for instance, that the oscillator locks to a perturbation signal with an offset of 10 MHz if the corresponding amplitude is larger than $\sim 10^{-4}$ A (when the signal is locked the sideband level becomes 0 dB). This information is useful when designing the floor plan of a chip, since it may put additional requirements on the placement (and shielding) of components that generate, or are sensitive to, perturbing signals.

4. MUTUAL INDUCTIVE COUPLING

Next we consider the two mutually coupled LC oscillators shown in Fig. 3. The inductive coupling between these two oscillators can be modeled as

$$(6a) \quad L_1 \frac{di_1(t)}{dt} + M \frac{di_2(t)}{dt} = v_1(t),$$

$$(6b) \quad L_2 \frac{di_2(t)}{dt} + M \frac{di_1(t)}{dt} = v_2(t),$$

where $M = k\sqrt{L_1 L_2}$ is the mutual inductance and $|k| < 1$ is the coupling factor. This makes the matrix

$$\begin{pmatrix} L_1 & M \\ M & L_2 \end{pmatrix}$$

positive definite, which ensures that the problem is well posed. In this section all the parameters with a subindex refer to the parameters of the oscillator with the same subindex. If we combine the mathematical model (5) of each oscillator with (6), then the two inductively coupled oscillators can be described by the following differential equations

$$(7a) \quad C_1 \frac{dv_1(t)}{dt} + \frac{v_1(t)}{R_1} + i_1(t) + S \tanh\left(\frac{G_n}{S} v_1(t)\right) = 0,$$

$$(7b) \quad L_1 \frac{di_1(t)}{dt} - v_1(t) = -M \frac{di_2(t)}{dt},$$

$$(7c) \quad C_2 \frac{dv_2(t)}{dt} + \frac{v_2(t)}{R_2} + i_2(t) + S \tanh\left(\frac{G_n}{S} v_2(t)\right) = 0,$$

$$(7d) \quad L_2 \frac{di_2(t)}{dt} - v_2(t) = -M \frac{di_1(t)}{dt}.$$

For small values of the coupling factor k the right-hand side of (7b) and (7d) can be considered as a small perturbation to the corresponding oscillator and we can apply the phase shift theory described in Section 2. Then we obtain the following simple nonlinear equations for the phase shift of each oscillator:

$$(8a) \quad \dot{\alpha}_1(t) = \mathbf{V}_1^T(t + \alpha_1(t)) \cdot \begin{pmatrix} 0 \\ -M \frac{di_2(t)}{dt} \end{pmatrix},$$

$$(8b) \quad \dot{\alpha}_2(t) = \mathbf{V}_2^T(t + \alpha_2(t)) \cdot \begin{pmatrix} 0 \\ -M \frac{di_1(t)}{dt} \end{pmatrix},$$

where the currents and voltages are evaluated by using (3):

$$(8c) \quad [v_1(t), i_1(t)]^T = \mathbf{x}_{ps}^1(t + \alpha_1(t)),$$

$$(8d) \quad [v_2(t), i_2(t)]^T = \mathbf{x}_{ps}^2(t + \alpha_2(t)).$$

4.1. Time discretization. The system (8) is solved by using implicit backward Euler for the time discretization and the Newton method is applied for the solution

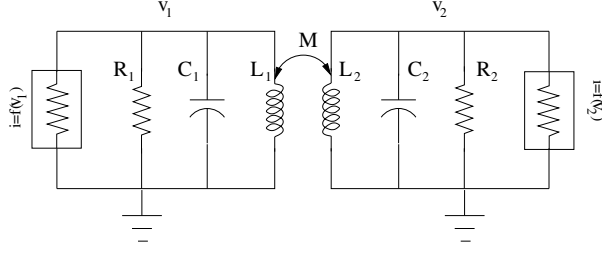


FIGURE 3. Two inductively coupled LC oscillators.

of the resulting two dimensional nonlinear equations (9a) and (9b), i.e.

$$(9a) \quad \alpha_1^{m+1} = \alpha_1^m + \tau \mathbf{V}_1^T (t^{m+1} + \alpha_1^{m+1}).$$

$$(9b) \quad \begin{pmatrix} 0 \\ -M \frac{i_2(t^{m+1}) - i_2(t^m)}{\tau} \end{pmatrix},$$

$$(9c) \quad \alpha_2^{m+1} = \alpha_2^m + \tau \mathbf{V}_2^T (t^{m+1} + \alpha_2^{m+1}).$$

$$(9d) \quad \begin{pmatrix} 0 \\ -M \frac{i_1(t^{m+1}) - i_1(t^m)}{\tau} \end{pmatrix},$$

$$(9e) \quad [v_1(t^{m+1}), i_1(t^{m+1})]^T = \mathbf{x}_{ps}^1(t^{m+1} + \alpha_1^{m+1}),$$

$$(9f) \quad [v_2(t^{m+1}), i_2(t^{m+1})]^T = \mathbf{x}_{ps}^2(t^{m+1} + \alpha_2^{m+1}),$$

$$\alpha_1^1 = 0, \alpha_2^1 = 0, m = 1, \dots,$$

where $\tau = t^{m+1} - t^m$ denotes the time step. For the Newton iterations in (9a) and (9b) we take (α_1^m, α_2^m) as initial guess on the time level $(m+1)$. This provides very fast convergence (in our applications within around four Newton iterations). See [4] and references therein for more details on time integration of electric circuits.

5. RESISTIVE AND CAPACITIVE COUPLING

For completeness in this section we describe how the phase noise theory applies to two oscillators coupled by a resistor or a capacitor.

5.1. Resistive coupling. Resistive coupling is modeled by connecting two oscillators by a single resistor, see Fig. 4. The current i_{R_0} flowing through the resistor R_0 satisfies the following relation

$$(10) \quad i_{R_0} = \frac{v_1 - v_2}{R_0},$$

where R_0 is the coupling resistance. Then the phase macromodel is given by

$$(11a) \quad \dot{\alpha}_1(t) = \mathbf{V}_1^T(t + \alpha_1(t)) \cdot \begin{pmatrix} (v_1 - v_2)/R_0 \\ 0 \end{pmatrix},$$

$$(11b) \quad \dot{\alpha}_2(t) = \mathbf{V}_2^T(t + \alpha_2(t)) \cdot \begin{pmatrix} -(v_1 - v_2)/R_0 \\ 0 \end{pmatrix},$$

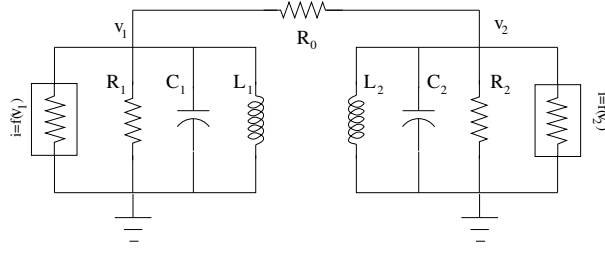


FIGURE 4. Two resistively coupled LC oscillators.

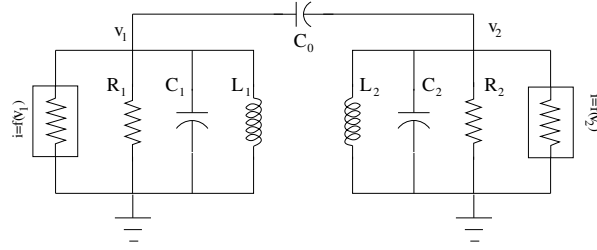


FIGURE 5. Two capacitively coupled LC oscillators.

where the voltages are updated by using (3). More details on resistively coupled oscillators can be found in [15].

5.2. Capacitive coupling. When two oscillators are coupled via a single capacitor with a capacitance C_0 (see Fig. 5), then the current i_{C_0} through the capacitor C_0 satisfies

$$(12) \quad i_{C_0} = C_0 \frac{d(v_1 - v_2)}{dt}.$$

In this case the phase macromodel is given by

$$(13a) \quad \dot{\alpha}_1(t) = \mathbf{V}_1^T(t + \alpha_1(t)) \cdot \begin{pmatrix} C_0 \frac{d(v_1 - v_2)}{dt} \\ 0 \end{pmatrix},$$

$$(13b) \quad \dot{\alpha}_2(t) = \mathbf{V}_2^T(t + \alpha_2(t)) \cdot \begin{pmatrix} -C_0 \frac{d(v_1 - v_2)}{dt} \\ 0 \end{pmatrix},$$

where the voltages are updated by using (3).

Time discretization of (11) and (13) is done according to (9).

6. OSCILLATOR COUPLING WITH BALUN

In this section we analyze inductive coupling effects between an oscillator and a balun. A balun is an electrical transformer that can transform balanced signals to unbalanced signals and vice versa, and they are typically used to change impedance (applications in (RF) radio). The (unintended) coupling between an oscillator and a balun typically occurs on chips that integrate several oscillators for, for instance,

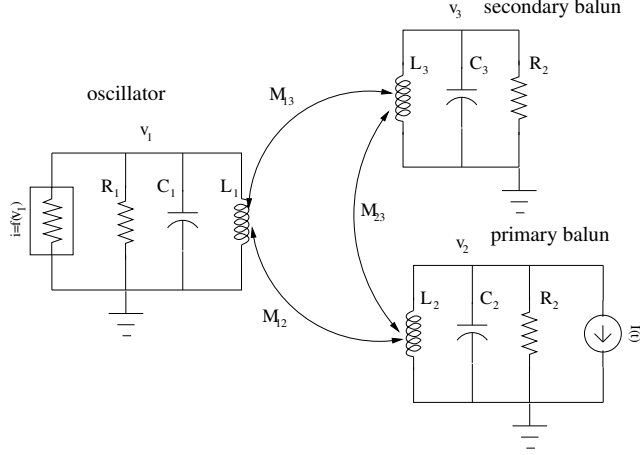


FIGURE 6. Oscillator coupled with a balun.

FM radio, Bluetooth and GPS, and hence it is important to understand possible coupling effects during the design. In Figure 6 a schematic view is given of an oscillator which is coupled with a balun via mutual inductors.

The following mathematical model is used for oscillator and balun coupling (see Fig. 6):

$$(14a) \quad C_1 \frac{dv_1(t)}{dt} + \frac{v_1(t)}{R_1} + i_1(t) + S \tanh\left(\frac{Gn}{S} v_1(t)\right) = 0,$$

$$(14b) \quad L_1 \frac{di_1(t)}{dt} + M_{12} \frac{di_2(t)}{dt} + M_{13} \frac{di_3(t)}{dt} - v_1(t) = 0,$$

$$(14c) \quad C_2 \frac{dv_2(t)}{dt} + \frac{v_2(t)}{R_2} + i_2(t) + I(t) = 0,$$

$$(14d) \quad L_2 \frac{di_2(t)}{dt} + M_{12} \frac{di_1(t)}{dt} + M_{23} \frac{di_3(t)}{dt} - v_2(t) = 0,$$

$$(14e) \quad C_3 \frac{dv_3(t)}{dt} + \frac{v_3(t)}{R_3} + i_3(t) = 0,$$

$$(14f) \quad L_3 \frac{di_3(t)}{dt} + M_{13} \frac{di_1(t)}{dt} + M_{23} \frac{di_2(t)}{dt} - v_3(t) = 0,$$

where $M_{ij} = k_{ij} \sqrt{L_i L_j}$, $i, j = 1, 2, 3$, $i < j$ is the mutual inductance and k_{ij} is the coupling factor. The parameters of the nonlinear resistor are $S = 1/R_1$ and $Gn = -1.1/R_1$ and the current injection in the primary balun is denoted by $I(t)$.

For small coupling factors we can consider $M_{12} \frac{di_2(t)}{dt} + M_{13} \frac{di_3(t)}{dt}$ in (14b) as a small perturbation to the oscillator. Then similar to (8), we can apply the phase shift macromodel to (14a)–(14b). The reduced model corresponding to (14a)–(14b) is

$$(15) \quad \frac{d\alpha(t)}{dt} = \mathbf{V}^T(t + \alpha(t)) \cdot \begin{pmatrix} 0 \\ -M_{12} \frac{di_2(t)}{dt} - M_{13} \frac{di_3(t)}{dt} \end{pmatrix}.$$

The balun is described by a linear circuit (14c)–(14d) which can be written in a more compact form:

$$(16) \quad E \frac{d\mathbf{x}(t)}{dt} + A\mathbf{x}(t) + B \frac{di_1(t)}{dt} + C = 0,$$

where

$$(17a) \quad E = \begin{pmatrix} C_2 & 0 & 0 & 0 \\ 0 & L_2 & 0 & M_{23} \\ 0 & 0 & C_3 & 0 \\ 0 & M_{23} & 0 & L_3 \end{pmatrix},$$

$$(17b) \quad A = \begin{pmatrix} 1/R_2 & 1 & 0 & 0 \\ -1 & 0 & 0 & 0 \\ 0 & 0 & 1/R_3 & 0 \\ 0 & 0 & -1 & 0 \end{pmatrix},$$

$$(17c) \quad B^T = (0 \quad M_{12} \quad 0 \quad M_{13}),$$

$$(17d) \quad C^T = (I(t) \quad 0 \quad 0 \quad 0),$$

$$(17e) \quad \mathbf{x}^T = (v_2(t) \quad i_2(t) \quad v_3(t) \quad i_3(t)).$$

With these notations (15) and (16) can be written in the following form

$$(18) \quad \frac{d\alpha(t)}{dt} = \mathbf{V}^T(t + \alpha(t)) \cdot \left(-B^T \frac{d\mathbf{x}(t)}{dt} \right),$$

$$(19) \quad E \frac{d\mathbf{x}(t)}{dt} + A\mathbf{x}(t) + B \frac{di_1(t)}{dt} + C = 0,$$

where $i_1(t)$ is computed by using (3). This system can be solved by using a finite difference method.

7. NUMERICAL EXPERIMENTS

It is known that a perturbed oscillator either locks to the injected signal or is pulled, in which case side band frequencies all fall on one side of the injected signal, see, e.g. [14]. It is interesting to note that contrary to the single oscillator case, where side band frequencies all fall on one side of the injected signal, for (weakly) coupled oscillators a double-sided spectrum is formed.

In Section 7.1–7.3 we consider two LC oscillators with different kinds of coupling and injection. The inductance and resistance in both oscillators are $L_1 = L_2 = 0.64 \text{ nH}$ and $R_1 = R_2 = 50 \Omega$, respectively. The first oscillator is designed to have a free running frequency $f_1 = 4.8 \text{ GHz}$ with capacitance $C_1 = 1/(4L_1\pi^2 f_1^2)$. Then the inductor current in the first oscillator is $A_1 = 0.0303 \text{ A}$ and the capacitor voltage is $V_1 = 0.5844 \text{ V}$. In a similar way the second oscillator is designed to have a free running frequency $f_2 = 4.6 \text{ GHz}$ with the inductor current $A_2 = 0.0316 \text{ A}$ and the capacitor voltage $V_2 = 0.5844 \text{ V}$. For both oscillators we choose $S_i = 1/R_i$, $G_n = -1.1/R_i$ with $i = 1, 2$.

In Section 7.4 we describe experiments for an oscillator coupled to a balun. In all the numerical experiments the simulations are run until $T_{\text{final}} = 6 \cdot 10^{-7} \text{ s}$ with the fixed time step $\tau = 10^{-11}$. Simulation results with the phase shift macromodel are compared with simulations of the full circuit using the CHORAL[7, 18] one-step time integration algorithm, hereafter referred to as full simulation. All experiments have been carried out in Matlab 7.3. We would like to remark that in all experiments

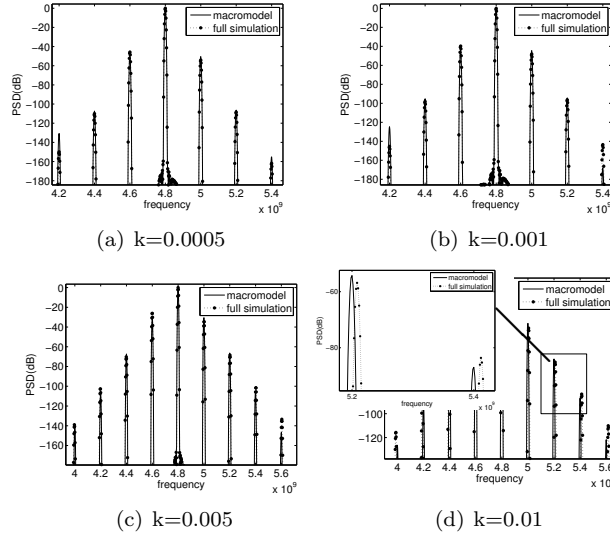


FIGURE 7. Inductive coupling. Comparison of the output spectrum obtained by the phase macromodel and by the full simulation for a different coupling factor k .

simulations with the macromodels were typically ten times faster than the full circuit simulations.

7.1. Inductively coupled oscillators. Numerical simulation results of two inductively coupled oscillators for different coupling factors k are shown in Fig. 7. For small values of the coupling factor we observe a very good approximation with the full simulation results. As the coupling factor grows, small deviations in the frequency occur, see Fig. 7(d). Because of the mutual pulling effects between the two oscillators a double sided spectrum is formed around each oscillator carrier frequency. The additional sidebands are equally spaced by the frequency difference of the two oscillators.

The phase shift $\alpha_1(t)$ of the first oscillator for a certain time interval is given in Fig. 8. We note that it has a sinusoidal behavior. Recall that for a single oscillator under perturbation a completely different behavior is observed: in locked condition the phase shift changes linearly, whereas in the unlocked case the phase shift has a nonlinear behavior different than a sinusoidal, see for example [13].

7.2. Capacitively coupled oscillators. The coupling capacitance in Fig. 5 is chosen to be $C_0 = k \cdot C_{\text{mean}}$, where $C_{\text{mean}} = (C_1 + C_2)/2 = 1.794 \cdot 10^{-12}$ and we call k the capacitive coupling factor. In Fig. 9 the numerical results are given for different capacitive coupling factors k . For larger values of the coupling factor the phase shift macromodel is not accurate enough and from Fig. 9(d) it is clear that the side band frequencies obtained by the phase macromodel differ from the full simulation results around 8 MHz (as expected).

The phase shift $\alpha_1(t)$ of the first oscillator and a zoomed section for some interval is given in Fig. 10. In a long run the phase shift seems to change linearly with the

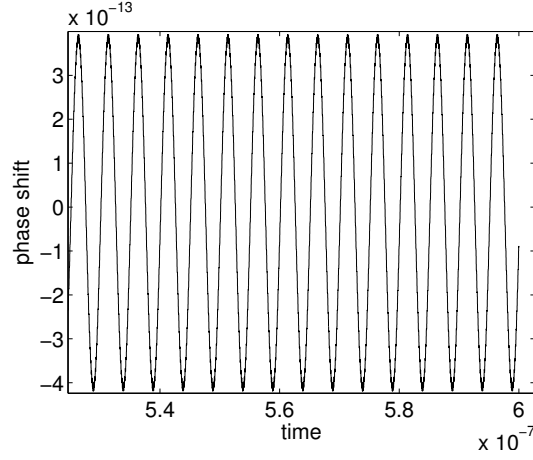


FIGURE 8. Inductive coupling. Phase shift $\alpha_1(t)$ of the first oscillator with $k=0.001$.

slope of $a = -0.00052179$. The linear change in the phase shift is a clear indication that the frequency of the first oscillator is changed and is locked to a new frequency, which is equal to $(1+a)f_1$. The change of the frequency can be explained as follows: as noted in [16], capacitive coupling may change the free running frequency because this kind of coupling changes the equivalent tank capacitance. From a mathematical point of view it can be explained in the following way. For the capacitively coupled oscillators the governing equations can be written as:

$$(20a) \quad (C_1 + C_0) \frac{dv_1(t)}{dt} + \frac{v_1(t)}{R} + i_1(t) + S \tanh\left(\frac{G_n}{S} v_1(t)\right) = C_0 \frac{dv_2(t)}{dt},$$

$$(20b) \quad L_1 \frac{di_1(t)}{dt} - v_1(t) = 0,$$

$$(20c) \quad (C_2 + C_0) \frac{dv_2(t)}{dt} + \frac{v_2(t)}{R} + i_2(t) + S \tanh\left(\frac{G_n}{S} v_2(t)\right) = C_0 \frac{dv_1(t)}{dt},$$

$$(20d) \quad L_2 \frac{di_2(t)}{dt} - v_2(t) = 0.$$

It shows that the capacitance in each oscillator is changed by C_0 and the new frequency of each oscillator is

$$\tilde{f}_i = \frac{1}{2\pi\sqrt{L_i(C_i + C_0)}}, \quad i = 1, 2.$$

In the zoomed figure within Fig.10 we note that the phase shift is not exactly linear but that there are small wiggles. By numerical experiments it can be shown that these small wiggles are caused by a small sinusoidal contribution to the linear part of the phase shift. As in case of mutually coupled inductors, the small sinusoidal

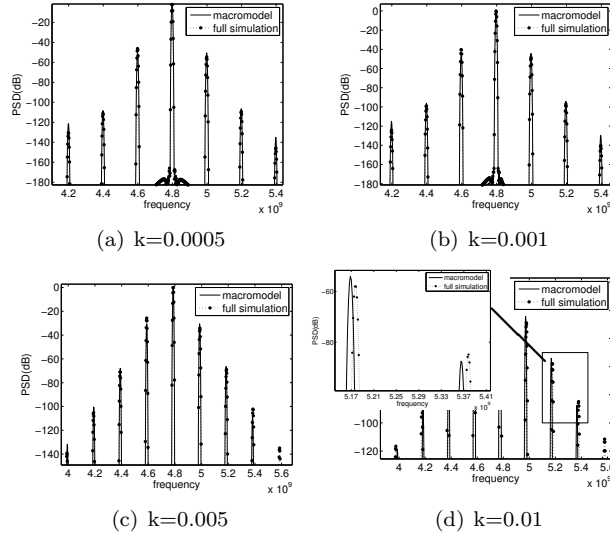


FIGURE 9. Capacitive coupling. Comparison of the output spectrum obtained by the phase macromodel and by the full simulation for a different coupling factor k .

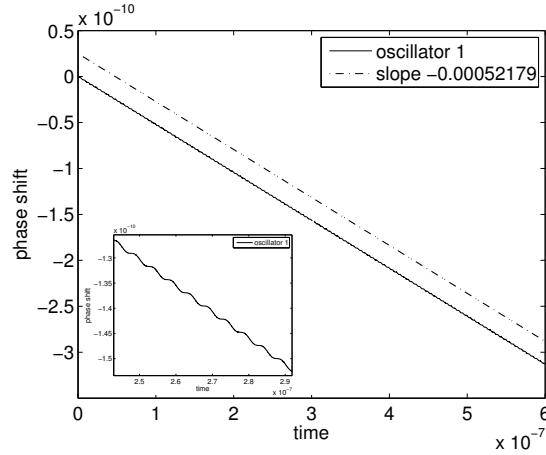


FIGURE 10. Capacitive coupling. Phase shift of the first oscillator with $k=0.001$.

contributions are caused by mutual pulling of the oscillators (right-hand side terms in (20a) and (20c)).

7.3. Inductively coupled oscillators under injection. As a next example, let us consider two inductively coupled oscillators where in one of the oscillators an injected current is applied. Let us consider a case when a sinusoidal current of the form

$$(21) \quad I(t) = A \sin(2\pi(f_1 - f_{\text{off}})t)$$

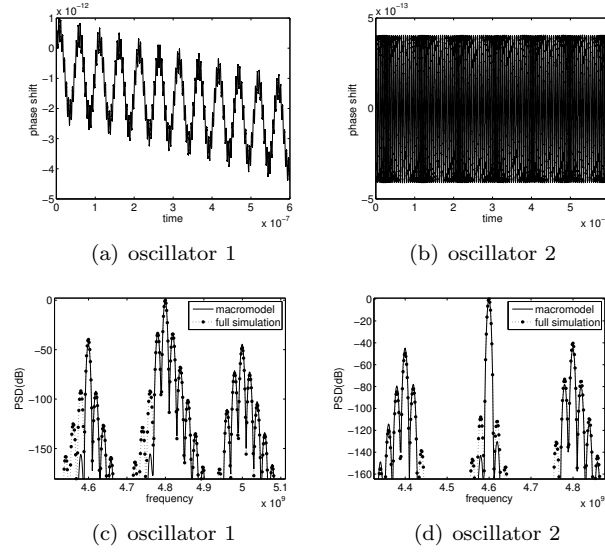


FIGURE 11. Inductive coupling with injection and $k = 0.001$. Top: phase shift. Bottom: comparison of the output spectrum obtained by the phase macromodel and by the full simulation with a small current injection.

is injected in the first oscillator. Then (8a) is modified to

$$(22) \quad \dot{\alpha}_1(t) = \mathbf{V}_1^T(t + \alpha_1(t)) \cdot \begin{pmatrix} -I(t) \\ -M \frac{di_2(t)}{dt} \end{pmatrix}.$$

For a small current injection with $A = 10 \mu\text{A}$ and an offset frequency $f_{\text{off}} = 20 \text{ MHz}$ the spectrum of the both oscillators with the coupling factor $k = 0.001$ is given in Fig.11. We observe that the phase macromodel is a good approximation of the full simulation results.

7.4. Oscillator coupled to a balun. Finally, consider an oscillator coupled to a balun as shown in Fig. 6 with the following parameters values:

Oscillator	Primary Balun	Secondary Balun
$L_1 = 0.64 \cdot 10^{-9}$	$L_2 = 1.10 \cdot 10^{-9}$	$L_3 = 3.60 \cdot 10^{-9}$
$C_1 = 1.71 \cdot 10^{-12}$	$C_2 = 4.00 \cdot 10^{-12}$	$C_3 = 1.22 \cdot 10^{-12}$
$R_1 = 50$	$R_2 = 40$	$R_2 = 60$

The coefficients of the mutual inductive couplings are

$$(23) \quad k_{12} = 10^{-3}, k_{13} = 5.96 * 10^{-3}, k_{23} = 9.33 * 10^{-3}.$$

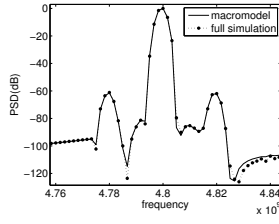
The injected current in the primary balun is of the form

$$(24) \quad I(t) = A \sin(2\pi(f_0 - f_{\text{off}})t),$$

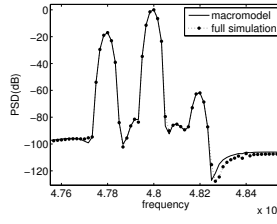
where $f_0 = 4.8 \text{ GHz}$ is the oscillator's free running frequency and f_{off} is the offset frequency.

Results of numerical experiments done with the phase macromodel and the full simulations are shown in Fig. 12. We note that for a small current injection both

$$A = 10^{-4}$$

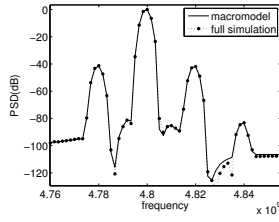


(a) oscillator

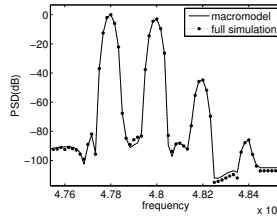


(b) primary balun

$$A = 10^{-3}$$

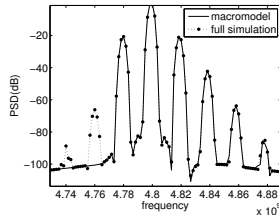


(c) oscillator

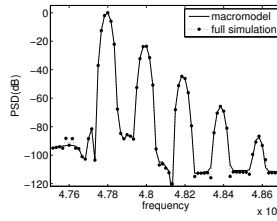


(d) primary balun

$$A = 10^{-2}$$

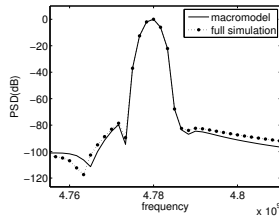


(e) oscillator

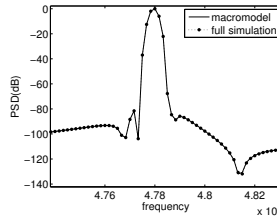


(f) primary balun

$$A = 10^{-1}$$



(g) oscillator



(h) primary balun

FIGURE 12. Comparison of the output spectrum of the oscillator coupled to a balun obtained by the phase macromodel and by the full simulation for an increasing injected current amplitude A and an offset frequency $f_{\text{off}} = 20$ MHz.

the oscillator and the balun are pulled by each other. For the injected current with $A = 10^{-1}$ both oscillator and balun are locked to the injected signal, see Fig. 12(g) and Fig. 12(h). Similar results are also obtained for the secondary balun.

8. CONCLUSION

In this paper we have shown how nonlinear phase macromodels can be used to accurately predict the behavior of individual or mutually coupled voltage controlled oscillators under perturbation, and how they can be used during the design process. Several types of coupling (resistive, capacitive, and inductive) have been described and for small perturbations, the nonlinear phase macromodels produce results with accuracy comparable to full circuit simulations, but at much lower computational costs. Furthermore, we have studied the (unintended) coupling between an oscillator and a balun, a case which typically arises during design and floor planning of RF circuits.

ACKNOWLEDGMENT

We would like to thank Jan-peter Frambach (STN-Wireless) for many helpful discussions about voltage- and digitally controlled oscillators. Marcel Hanssen (NXP Semiconductors) provided us measurement data for the inductor and capacitors. For the CHORAL implementation we thank Michael Striebel from the University of Chemnitz.

REFERENCES

- [1] R. Adler. A study of locking phenomena in oscillators. *Proc. of the I.R.E. and waves and electrons*, 34:351–357, June 1946.
- [2] S. Agarwal and J. Roychowdhury. Efficient multiscale simulation of circadian rhythms using automated phase macromodelling techniques. In *Proc. Pacific Symposium on Biocomputing*, volume 13, pages 402–413, 2008.
- [3] A. Banai and F. Farzaneh. Locked and unlocked behaviour of mutually coupled microwave oscillators. In *IEE Proc. Antennas and Propagation*, volume 147, pages 13–18, 2000.
- [4] P. G. Ciarlet, W. H. A. Schilders, and E. J. W. ter Maten, editors. *Numerical Methods in Electromagnetics*, volume 13 of *Handbook of Numerical Analysis*. Elsevier, 2005.
- [5] A. Demir, D. Long, and J. Roychowdhury. Computing phase noise eigenfunctions directly from steady-state jacobian matrices. *Computer Aided Design, 2000. ICCAD-2000. IEEE/ACM International Conference on*, pages 283–288, 2000.
- [6] A. Demir, A. Mehrotra, and J. Roychowdhury. Phase noise in oscillators: a unifying theory and numerical methods for characterization. *IEEE Trans. Circ. Syst. I*, 47(5):655–674, May 2000.
- [7] M. Günther. Simulating digital circuits numerically – a charge-oriented ROW approach. *Numer. Math.*, 79:203–212, 1998.
- [8] M. Günther, U. Feldmann, and J. ter Maten. Modelling and discretization of circuit problems. In *Handbook of numerical analysis. Vol. XIII, Handb. Numer. Anal., XIII*, pages 523–659. North-Holland, Amsterdam, 2005.
- [9] M. E. Heidari and A. A. Abidi. Behavioral models of frequency pulling in oscillators. In *IEEE Int. Behavioral Modeling and Simulation Workshop*, pages 100–104, 2007.
- [10] S. H. J. M. Houben. *Circuits in motion: the numerical simulation of electrical oscillators*. PhD thesis, Technische Universiteit Eindhoven, 2003.
- [11] T. A. M. Kevenaer. Periodic steady state analysis using shooting and wave-form-Newton. *Int. J. Circ. Theory Appls*, 22(1):51–60, 1994.
- [12] K. Kundert, J. White, and A. Sangiovanni-Vincentelli. An envelope-following method for the efficient transient simulation of switching power and filter circuits. *Computer-Aided Design, 1988. ICCAD-88. Digest of Technical Papers., IEEE International Conference on*, pages 446–449, Nov 1988.

- [13] X. Lai and J. Roychowdhury. Automated oscillator macromodelling techniques for capturing amplitude variations and injection locking. *Computer Aided Design, 2004. ICCAD-2004. IEEE/ACM International Conference on*, pages 687–694, Nov. 2004.
- [14] X. Lai and J. Roychowdhury. Capturing oscillator injection locking via nonlinear phase-domain macromodels. *IEEE Trans. Micro. Theory Tech.*, 52(9):2251–2261, September 2004.
- [15] X. Lai and J. Roychowdhury. Fast and accurate simulation of coupled oscillators using nonlinear phase macromodels. In *Microwave Symposium Digest, 2005 IEEE MTT-S International*, pages 871–874, 2005.
- [16] X. Lai and J. Roychowdhury. Fast simulation of large networks of nanotechnological and biochemical oscillators for investigating self-organization phenomena. In *Proc. IEEE Asia South-Pacific Design Automation Conference*, pages 273–278, 2006.
- [17] B. Razavi. A study of injection locking and pulling in oscillators. *IEEE J. Solid-State Circ.*, 39(9):1415–1424, September 2004.
- [18] P. Rentrop, M. Günther, M. Hoschek, and U. Feldmann. CHORAL—a charge-oriented algorithm for the numerical integration of electrical circuits. In *Mathematics—key technology for the future*, pages 429–438. Springer, Berlin, 2003.
- [19] A. Semlyen and A. Medina. Computation of the periodic steady state in systems with nonlinear components using a hybrid time and frequency domain method. *IEEE Trans. Power Syst.*, 10(3):1498–1504, 1995.
- [20] Y. Wan, X. Lai, and J. Roychowdhury. Understanding injection locking in negative resistance lc oscillators intuitively using nonlinear feedback analysis. In *Proc. IEEE Custom Integrated Circuits Conference*, pages 729–732, 2005.

DEPARTMENT OF MATHEMATICS AND COMPUTER SCIENCE, CASA GROUP, TECHNISCHE UNIVERSITEIT EINDHOVEN, PO BOX 513, 5600 MB EINDHOVEN, THE NETHERLANDS.
E-mail address: [d.harutyunyan,e.j.w.ter.maten,w.h.a.schilders]@tue.nl

NXP SEMICONDUCTORS, CORPORATE I&T/DTF, HTC 37 WY4-01, 5656 AE EINDHOVEN, THE NETHERLANDS.
E-mail address: [joost.rommes, jan.ter.maten, wil.schilders]@nxp.com.